ACS APPLIED MATERIALS & INTERFACES

Research Article

Cite This: ACS Appl. Mater. Interfaces XXXX, XXX, XXX−XXX

www.acsami.org

Highly Sensitive and Reusable Membraneless Field-Effect Transistor (FET)-Type Tungsten Diselenide (WSe_2) Biosensors

Hae Won Lee,[†,⊥] Dong-Ho Kang,[‡,⊥] Jeong Ho Cho,[§] Sungjoo Lee,[‡,§] Dong-Hwan Jun,[*,∥] and Jin-Hong Park[*,†,‡,§]

[†]School of Semiconductor and Display Engineering, [‡]School of Electronic and Electrical Engineering, and [§]SKKU Advanced Institute of Nano Technology (SAINT), Sungkyunkwan University, Suwon 16419, Korea

[∥]Korea Advanced Nano Fab Center (KANC), Suwon 16229, Korea

Supporting Information

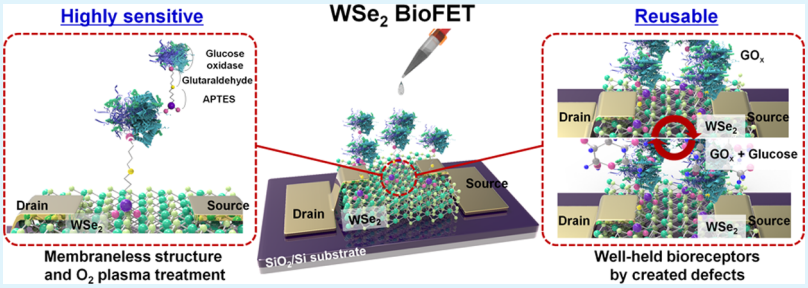

ABSTRACT: In recent years when the demand for high-performance biosensors has been aroused, a field-effect transistor (FET)-type biosensor (BioFET) has attracted great interest because of its high sensitivity, label-free detection, fast detection speed, and miniaturization. However, the insulating membrane in the conventional BioFET, which is essential in preventing the surface dangling bonds of typical semiconductors from nonspecific bindings, has limited the sensitivity of biosensors. Here, we present a highly sensitive and reusable membraneless BioFET based on a defect-free van der Waals material, tungsten diselenide (WSe_2). We intentionally generated a few surface defects that serve as extra binding sites for the bioreceptor immobilization through weak oxygen plasma treatment, consequently magnifying the sensitivity values to 2.87×10^5 A/A for 10 mM glucose. The WSe_2 BioFET also maintained its high sensitivity even after several cycles of rinsing and glucose application were repeated.

KEYWORDS: *BioFET, highly sensitive, reusable, membraneless structure, vdW material*

INTRODUCTION

In recent years, the demand for highly sensitive and reusable biosensors has increased because the applications based on biosensors have become diverse, with the range including medical, agricultural, industrial, and environmental fields.[1−4] To address this high-performance need, various types of biosensors such as electrochemical biosensors,[5−8] optical biosensors,[9−12] piezoelectric biosensors,[13−16] and electrical biosensors[17−20] have been proposed. In particular, the field-effect transistor (FET)-type biosensor (BioFET) has attracted great interest because of its high sensitivity, label-free detection, fast detection speed, and miniaturization. The concept of BioFETs was first introduced by P. Bergveld in 1970[19] with a simple sensing mechanism that the adsorption of target biomolecules into bioreceptors on an insulating membrane directly modulates the channel conductance, consequently changing the drain current level. Conventional BioFETs have structure similar to that of metal−oxide−semiconductor FETs, where a bioreceptor layer is used instead of a metal gate on the insulating membrane. Although BioFETs based on typical semiconductors such as silicon (Si) can utilize the commercial complementary metal−oxide−semiconductor fabrication process, using a membrane hinders high sensitivity and reliability. The sensitivity of the BioFETs is strongly dependent on the thickness and dielectric constant of the insulating membrane because the membrane capacitance determines the sensing currents. In addition, the bulk defects in the membrane and the interface defects at the channel/membrane interface negatively affect the sensitivity and reliability of the BioFETs by causing irreversible current degradation, parasitic coupling, and the threshold voltage shift phenomenon.[21−24] However, the membrane-based structure is inevitable for conventional BioFETs owing to the countless surface detects of semiconductor materials. Unless a membrane is used, many surface dangling bonds not only react with the targeted biomolecules but also with nontargets (nonspecific bindings), thereby inducing noise and attenuating sensitivity.[25−27]

Here, we demonstrate a highly sensitive and reusable membraneless tungsten diselenide (WSe_2) BioFET, where the channel material WSe_2 is one of the transition metal

Received: February 28, 2018
Accepted: May 4, 2018

DOI: 10.1021/acsami.8b03432
ACS Appl. Mater. Interfaces XXXX, XXX, XXX−XXX

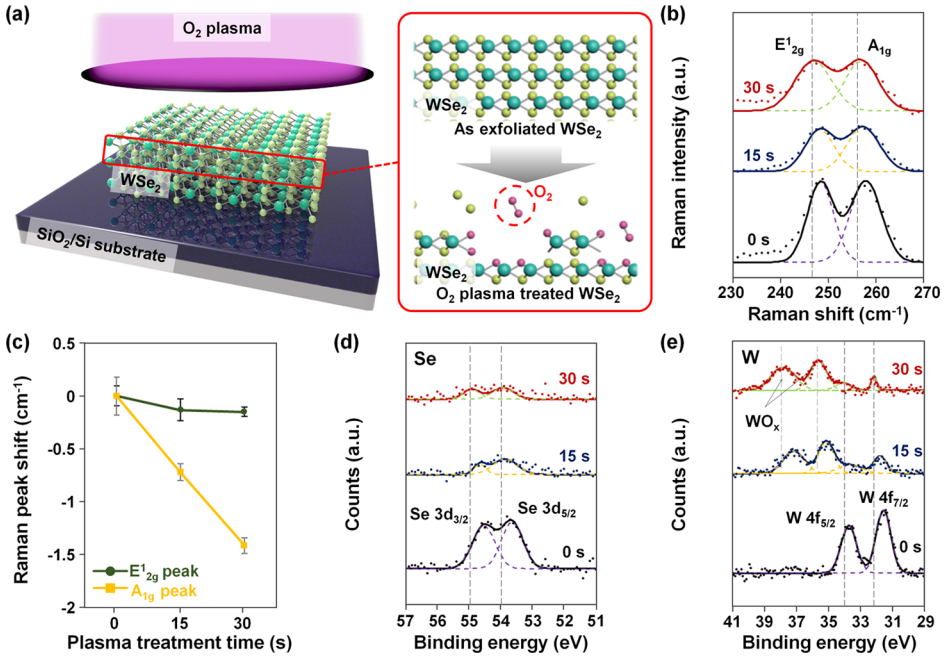

Figure 1. Effects of O_2 plasma treatment on WSe_2. (a) Schematic illustrations of O_2 plasma treatment on WSe_2. (b) Raman spectra of 0 s (black), 15 s (blue), and 30 s (red) plasma-treated WSe_2. (c) Extracted Raman peak shift values as a function of O_2 plasma treatment time. XPS spectra of (d) Se $3d_{3/2}$ and Se $3d_{5/2}$ and (e) W $4f_{5/2}$ and W $4f_{7/2}$ states.

dichalcogenides with a layered structure based on the van der Waals (vdW) interaction. The almost nonexistent defects on the WSe_2 surface without dangling bonds allow for the highly sensitive operation of the membraneless WSe_2-BioFETs, unaffected by the nonspecific binding. We generate only small amounts of defects that serve as binding sites for bioreceptors on the defect-free WSe_2 surface through weak oxygen (O_2) plasma, thereby maximizing the sensitivity of the WSe_2 BioFET. In the first part of this paper, we investigate the effects of the O_2 plasma process on WSe_2 by Raman spectroscopy and X-ray photoelectron spectroscopy (XPS). In the second part, we discuss the sensing performance and reusability of our WSe_2 BioFETs using glucose oxidase (GO_x) as the bioreceptor and glucose as the targeted biomolecules.

EXPERIMENTAL SECTION

O_2 Plasma Process on WSe_2. Mechanically exfoliated WSe_2 flakes were transferred onto 90 nm thick SiO_2 on a heavily boron-doped Si substrate. The O_2 plasma process was performed on the WSe_2 flakes using a plasma machine (Miniplasma Cube, Plasmart). For a 30 s treated sample, we repeated 15 s of treatment twice, with an interval of 5 s, to prevent severe damages or excessive etching on the flakes. The set conditions during the O_2 plasma treatment are as follows: reactive ion etcher power (20 W), plasma pressure (470 mTorr), and O_2 flow rates (5 sccm).

Characterization of Plasma-Treated and 3-Aminopropyl Triethoxysilane-Treated WSe_2. Raman spectroscopy (alpha300 M +, WITec) was used to analyze the effects of O_2 plasma treatment and 3-aminopropyl triethoxysilane (APTES) treatment on the WSe_2 flakes. In the Raman measurement, the excitation wavelength was 532 nm, with 2 nW power. The laser beam size was approximately 0.7−0.9 μm, and the instrumental spectral resolution was approximately 1 cm^{-1}. The WSe_2 samples were measured with an integration time of 5 s and the gratings of the spectrometer at 1800 g mm^{-1}. For the XPS (ESCA 200, VG Microtech Inc.) measurement, an Mg Kα twin-anode source was used with the X-ray incident angle of 0°.

Fabrication of Membraneless WSe_2 BioFET. The WSe_2 flakes with thickness of approximately 60 nm (Supporting Information Figure S1) were mechanically exfoliated and transferred onto 90 nm thick SiO_2 on a heavily boron-doped Si substrate. Subsequently, the source and drain electrodes (channel length and width of 5 μm) were patterned through optical lithography, followed by the deposition of Pt (10 nm) and Au (30 nm) layers using an e-beam evaporator. The fabricated back-gated WSe_2 devices underwent the surface treatment processes of O_2 plasma treatment and bioreceptor treatment.

Bioreceptor Treatment on WSe_2. To facilitate the interaction of the WSe_2 surface with biocomponents,[28] the WSe_2 region in BioFET was first modified with a common chemical linker APTES (0.5% in toluene) and the sample was dried at 120 °C for 30 min. Subsequently, for the specific and sensitive detection of targets (glucose), we immobilized the bioreceptors on the surface of the O_2 plasma-treated WSe_2 channel. The device was kept in a glutaraldehyde solution for 2 h, followed by a GO_x treatment (1% in phosphate-buffered saline, pH 7.4) at 4 °C for 10 h.

Electrical Characterization of Membraneless WSe_2 BioFET. The electrical sensing performance of the membraneless WSe_2 BioFET was analyzed using a Keysight B2912A semiconductor parameter analyzer. The glucose solution (target) in different concentrations (1, 5, and 10 mM in deionized (DI) water) was dropped onto the channel region, followed by the electrical measurements. The WSe_2 BioFET was reused after being rinsed in DI water to remove the targets. We measured the current−voltage characteristics (I_D−V_G) of the device before and after the O_2 plasma treatment, bioreceptor immobilization, and target adsorption. The sensitivity was extracted from the I_D−V_G data, and all drain currents were normalized by the channel width (W_{ch} = 5 μm).

RESULTS AND DISCUSSION

We performed O_2 plasma treatment for 15 and 30 s on WSe_2 flakes that were mechanically exfoliated onto an SiO_2/Si substrate, as shown in the schematic illustrations of Figure 1a. In particular, to create small amounts of defects while minimizing the severe crystallinity damage and excessive surface defects, we chose O_2 gas with a small kinetic energy (oxygen molecular mass 32 g mol^{-1}) and set a weak plasma power (20 W). The effect of the O_2 plasma treatment on WSe_2 semiconductor was then investigated by Raman spectroscopy

DOI: 10.1021/acsami.8b03432
ACS Appl. Mater. Interfaces XXXX, XXX, XXX−XXX

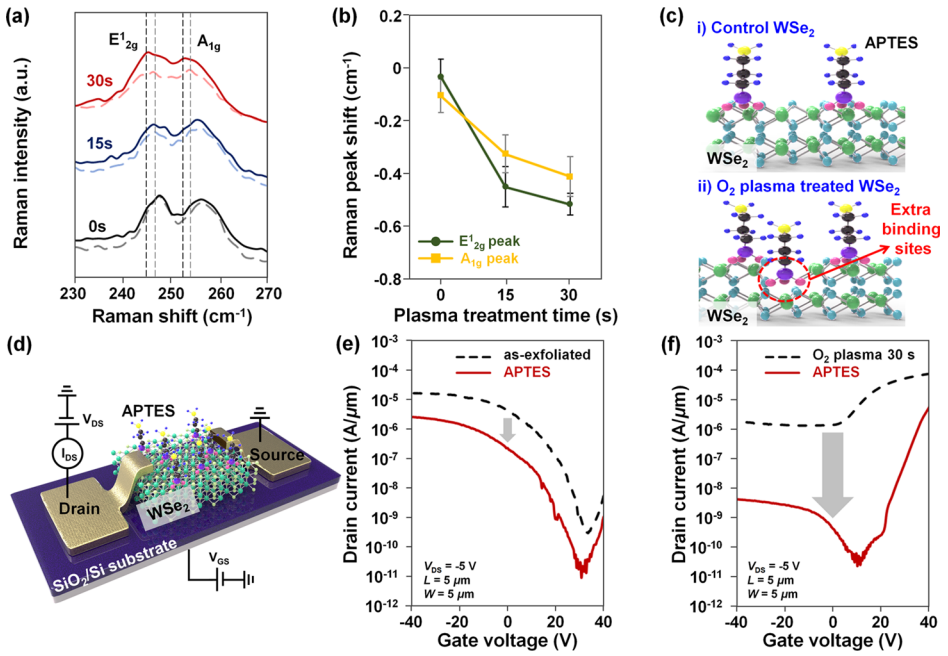

Figure 2. APTES treatment on O_2 plasma-treated and control WSe_2. (a) Raman spectra before (dotted line) and after (solid line) APTES treatment for 15 s (blue)/30 s (red) O_2 plasma-treated WSe_2 and control (black) WSe_2. (b) Extracted Raman peak shift values as a function of plasma treatment time. (c) Schematic illustrations showing APTES attachment on the O_2 plasma-treated and control WSe_2 surfaces. (d) Schematic illustrations of the WSe_2 BioFET on which APTES molecules were attached. I_D−V_G characteristics before (black dotted line) and after (red solid line) APTES attachment on (e) the control WSe_2 BioFET and (f) the plasma-treated WSe_2 BioFET.

and XPS (0, 15, and 30 s plasma-treated samples). As shown in the Raman spectra from Figure 1b, we confirmed that the conventional WSe_2 E^1_{2g} peak (in-plane vibration) and A_{1g} peak (out-plane vibration) were at 248.39 and 257.88 cm^{-1}, respectively, with full width at half-maximum (fwhm) values of 6.49 and 7.51 cm^{-1}, respectively, on the control WSe_2 sample (no plasma treatment). After the O_2 plasma treatment, the fwhm values of the E^1_{2g} peak and A_{1g} peak increased to 7.22 and 8.09 cm^{-1}, respectively, for the 15 s plasma-treated WSe_2 sample and to 9.14 and 8.37 cm^{-1}, respectively, for the 30 s plasma-treated WSe_2 sample. The increase in FWHM values indicates that the plasma process damaged the crystallinity of WSe_2 and that crystal defects were created on the surface, as we intended.[29−31] We also observed slightly red-shifted E^1_{2g} and A_{1g} peaks after O_2 plasma treatment to 248.21 and 257.34 cm^{-1}, respectively, for the 15 s plasma-treated sample and 246.89 and 256.27 cm^{-1}, respectively, for the 30 s plasma-treated sample. For a precise comparison, we extracted the Raman peak shift values from nine different samples after 15 and 30 s treatments based on O_2 plasma, where the measurement was performed at three different points in each sample (Figure 1c). After 15 s of O_2 plasma treatment, the E^1_{2g} and A_{1g} peaks shifted −0.13 and −0.72 cm^{-1}, respectively; after 30 s, the E^1_{2g} and A_{1g} peaks shifted −0.15 and −1.41 cm^{-1}, respectively. Previously reported works have shown that the red shift phenomenon is mostly induced by the n-doping effect.[32−34] We then performed XPS on the 0, 15, and 30 s plasma-treated samples to clarify the doping type and further investigate the surface modification of WSe_2 by O_2 plasma treatment. Figure 1d,e shows the XPS spectra of Se 3d and W 4f on WSe_2 before and after O_2 plasma treatments (15 s/30 s). In the control WSe_2 flakes, two distinctive peaks occurred at 54.54 and 53.65 eV, which represent the Se $3d_{3/2}$ and Se $3d_{5/2}$ states, respectively (Figure 1d). As the O_2 plasma treatment was applied, the Se $3d_{3/2}$ and Se $3d_{5/2}$ peaks slightly upshifted to 55.15 and 54.16 eV (30 s plasma-treated sample), respectively. The shift of the Se 3d peaks toward higher binding energies indicates the elevation in the WSe_2 Fermi level and the decrease in the work function (n-doping),[35,36] which is also coincident with the Raman analysis result. In addition, the Se 3d peaks attenuated after the O_2 plasma treatment as a result of the broken bonds between W and Se atoms and the generation of Se vacancies in WSe_2.[35,37] Similarly, the upshift phenomenon [W $4f_{5/2}$ peak from 33.60 eV (0 s) to 34.05 eV (30 s) and W $4f_{7/2}$ peak from 31.54 eV (0 s) to 32.14 eV (30 s)] and the attenuation of peaks after O_2 plasma treatment were also observed at W 4f peaks, as shown in Figure 1e. Furthermore, two extra peaks were presented in the O_2 plasma-treated W XPS spectra at 37.15 and 35.13 eV (15 s) and 37.80 and 35.60 eV (30 s), which did not exist in the control W XPS spectra. The new peaks are consistent with previously reported WO_x peaks at ≈37 and ≈35 eV,[31,37] which indicate the formation of W−O bonds. According to these XPS results, we speculated that the O_2 plasma treatment broke the W−Se bonds and subsequently generated Se vacancies and W−O bonds on the WSe_2 surface.

Next, to investigate how well the bioreceptors (glucose oxidase: GO_x) are immobilized on the WSe_2 surface after O_2 plasma treatment, we prepared the control, 15, and 30 s plasma-treated WSe_2 samples and incubated the samples in the APTES solution for 30 min. We then performed Raman analysis on the samples before and after the APTES treatment process. Here, a self-assembled organic material with amine ($-NH_2$) functional group, APTES, was served as a chemical linker to immobilize the GO_x bioreceptor molecules on the WSe_2 BioFET. Because of W−O bonds generated after the O_2 plasma treatment, more number of APTES molecules is expected to be attached on the WSe_2 surface as silanes attached well on the oxygen-rich surfaces.[38] Figure 2a shows the Raman

DOI: 10.1021/acsami.8b03432
ACS Appl. Mater. Interfaces XXXX, XXX, XXX−XXX

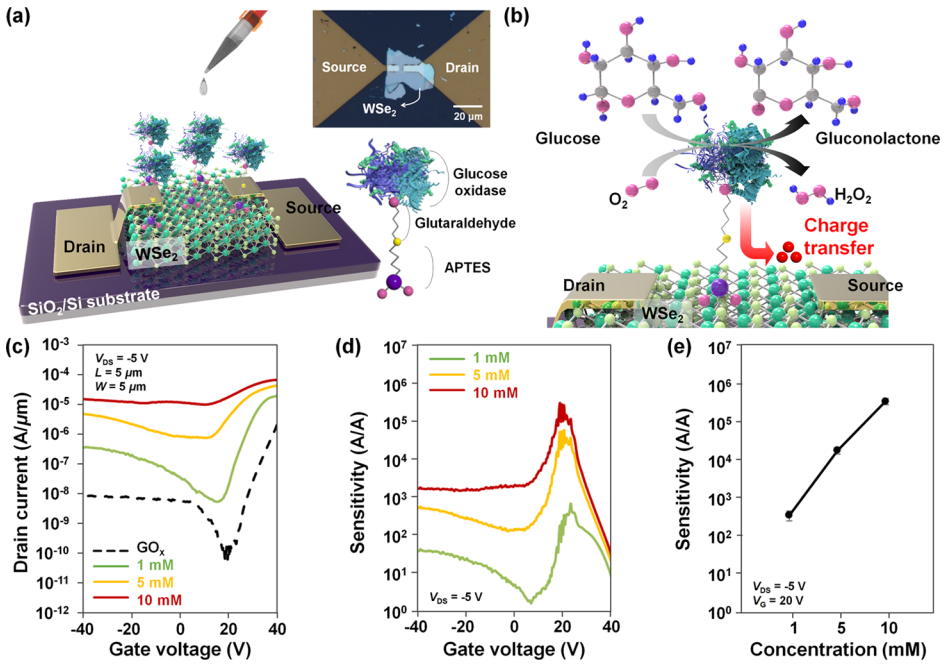

Figure 3. Glucose-sensing performance of the membraneless WSe_2 BioFET. (a) Schematic illustration and optical image of WSe_2 BioFET with GO_x bioreceptor. (b) Schematic illustrations explaining (i) redox reaction between glucose (target) and glucose oxidase (bioreceptor) and (ii) electron transfer to the WSe_2 channel surface. (c) I_D–V_G characteristics of the WSe_2 BioFET exposed to different concentrations (1, 5, and 10 mM) of glucose. (d) Sensitivity values as a function of gate voltage under different glucose concentrations. (e) Average sensitivity values obtained from five different devices as a function of glucose concentration.

spectra of the control, 15, and 30 s plasma-treated WSe_2 samples before (dotted lines) and after (solid lines) the APTES treatment. Conventional E^1_{2g} and A_{1g} WSe_2 peaks appeared around 247 and 256 cm^{-1}, respectively, from all samples (control, 15, and 30 s plasma-treated samples). After the APTES layer was coated on the WSe_2 surface, the red-shift phenomenon was observed in the Raman peaks because the negative poles of the $-NH_2$ molecules in APTES pushed the electrons away from the APTES/WSe_2 interface, thus inducing the n-doping phenomenon.[33,34] In particular, as the O_2 plasma process time increased, the Raman peak shift became more obvious compared to the control sample, in which negligible shifts were observed. We extracted the Raman peak shift values before and after APTES treatment from the control, 15, and 30 s plasma-treated samples (Figure 2b). In the control WSe_2 sample without O_2 plasma treatment, the E^1_{2g} peak and A_{1g} peak shifted only −0.03 and −0.10 cm^{-1}, respectively, after attaching the APTES molecules. The Raman peak shift values increased according to the O_2 plasma treatment time such that the E^1_{2g} and A_{1g} peaks, respectively, shifted −0.45 and −0.33 cm^{-1} after 15 s and shifted −0.52 and −0.41 cm^{-1} after 30 s. On the basis of these Raman analysis results, more APTES molecules are predicted to attach on the WSe_2 surface that was treated by the O_2 plasma process for a longer time (i.e., the surface has more crystal defects). The intentionally created surface defects on the plasma-treated WSe_2 surface are expected to serve as extra binding sites for holding the APTES molecules, as shown in the schematic illustrations of Figure 2c. To verify this prediction, we then fabricated a membraneless WSe_2 BioFET and analyzed the electrical characteristics on the control and the 30 s plasma-treated BioFETs. Figure 2d shows the schematic illustrations of the WSe_2 BioFET with the APTES chemical linkers. The electrical characteristics of the control and O_2 plasma-treated WSe_2 BioFETs are shown in Figure 2e,f, where the current values are normalized by the channel width. Figure 2e presents the drain current–gate voltage (I_D–V_G) characteristics of the control WSe_2 BioFET before (black dotted line) and after (red solid line) the APTES treatment. Because the WSe_2 channel was n-doped by APTES, the threshold voltage (Vth) shifts negatively and the current level decreased by a factor of 10 (at V_G = 0 V) after the APTES treatment. In Figure 2f, the plasma-treated BioFET also showed n-doped characteristics by the APTES molecules. In particular, the n-doping effect of the APTES molecules increased so much that the current level significantly decreased by a factor of 10^3 (at V_G = 0 V). This considerable decrement in current level indicates that the amount of APTES molecules attached on the surface of the WSe_2 channel is much greater at the plasma-treated BioFET than at the control device, which is also in agreement with the Raman analysis.

To investigate the sensing performance of the membraneless WSe_2 BioFET, the O_2 plasma-treated WSe_2 BioFETs underwent the surface functionalization process by applying APTES, glutaraldehyde (middle-linker), and GO_x (final bioreceptor). Figure 3a shows the schematic illustration and optical image of the WSe_2 BioFET with a drop of glucose (target). The WSe_2 BioFET senses the current change when GO_x interacts with glucose and the redox reaction occurs. GO_x on the surface of the WSe_2 channel oxidizes glucose to form gluconolactone, simultaneously reducing GO_x itself. Subsequently, GO_x is reoxidized by consuming O_2 as a mediator to form hydrogen peroxide (H_2O_2) as follows

$$\text{Glucose } (C_6H_{12}O_6) + \text{glucose oxidase}_{(ox)} \rightarrow \text{gluconolactone } (C_6H_{10}O_6) + \text{glucose oxidase (red)}$$

$$\text{Glucose oxidase}_{(red)} + O_2 \rightarrow \text{glucose oxidase}_{(ox)} + H_2O_2$$

DOI: 10.1021/acsami.8b03432
ACS Appl. Mater. Interfaces XXXX, XXX, XXX−XXX

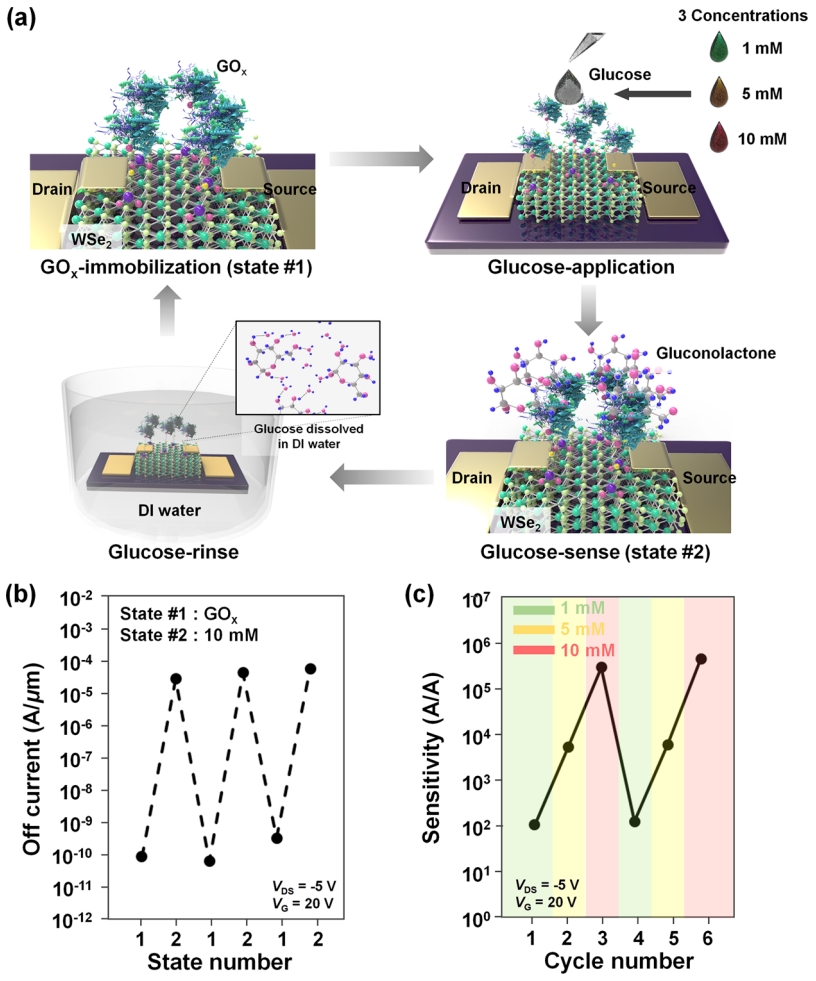

Figure 4. Reusability of the membraneless WSe_2 BioFET. (a) Schematic illustration for reusability experiment process. (b) Current values (at V_G = 20 V) in state #1 (GO_x) and state #2 (10 mM glucose) for three repeated cycles. (c) Sensitivity values extracted from six cycles with three (1, 5, 10 mM) glucose concentrations.

where glucose oxidase$_{(ox)}$ is the oxidized form of GO_x and glucose oxidase$_{(red)}$ is the reduced form of GO_x.[5−7] In these chemical reactions, electrons are produced and directly transferred to the WSe_2 channel owing to the membraneless structure, as depicted in Figure 3b. The electrical characteristics (I_D−V_G characteristics) of the WSe_2 BioFET were examined with three different concentrations of glucose (1 mM (green line), 5 mM (yellow line), and 10 mM (red line) in DI water) in Figure 3c. The chosen concentrations were in the range between 1 and 10 mM, which is known as the glucose concentration range in the human body. The black dotted line represents the current level of the WSe_2 BioFET with the receptor GO_x immobilized on the channel surface. After dropping the glucose solution on the channel, the overall current level increased as the electrons generated from the redox reaction were transferred onto the WSe_2 channel, consequently increasing the channel conductivity. The redox reaction, which becomes more active in proportion to the glucose concentrations, seems to make the current level to gradually increase according to the glucose concentrations. We then calculated the sensitivity values defined as the ratio of the current difference between the sensing (glucose-dropped state) and the base current (GO_x-immobilized state) to the base current value $[(I_{sensing} - I_{base})/I_{base}]$. The extracted sensitivity values are shown as a function of gate voltage in Figure 3d. For all concentrations, the largest sensitivity values appeared at around V_G = 20 V because the base current is the lowest at V_G = 20 V. Here, we achieved an extremely high sensitivity of 6.99 × 10^2 A/A for 1 mM, 5.76 × 10^4 A/A for 5 mM, and 2.87 × 10^5 A/A for 10 mM. In addition, we investigated the sensing performance for each condition with five different WSe_2 BioFET devices to evaluate the reliability of this experiment. In Figure 3e, the average sensitivity values extracted from the devices are shown with error bars as a function of glucose concentration. The average sensitivity values were 3.47 × 10^2 A/A, 1.58 × 10^4 A/A, and 2.86 × 10^5 A/A for 1, 5, and 10 mM, respectively, which showed approximately 20% of device-to-device variations at V_G = 20 V. In spite of these variations in sensitivity, the increasing tendency in the sensitivity values was obvious according to the glucose concentration increased.

Finally, we examined the reusability of the membraneless WSe_2 BioFET by monitoring its sensing performance while sensing and rinsing glucose repeatedly. The Figure 4a shows the overall process for the reusability experiment, where the "bioreceptor GO_x-immobilized state" is named as state #1 and the "target glucose-sensed state" as state #2. With the WSe_2 BioFET in which the GO_x immobilization process had finished, we measured its electrical performance before (state #1) and after (state #2) dropping the glucose solution onto the WSe_2 channel region. Subsequently, the WSe_2 BioFET was rinsed in

DOI: 10.1021/acsami.8b03432
ACS Appl. Mater. Interfaces XXXX, XXX, XXX−XXX

DI water and reverted to the device state before sensing glucose, where only the bioreceptor GO_x was left on the channel (state #1). These series of processes was regarded as one cycle, and this cycle was repeated several times to see if the WSe_2 BioFET is reusable. After we confirmed the thorough removal of glucose and the return to state #1 by the rinsing step in Supporting Information Figure S2, we repeated several cycles of the application and rinsing of glucose processes on the device and we measured the electrical characteristic at each step. Figure 4b presents the current values extracted at V_G = 20 V after GO_x was immobilized (state #1) and 10 mM glucose was applied (state #2) on the channel. The current increased from 9.76×10^{-11} A/μm (state #1) to 2.81×10^{-5} A/μm (state #2) owing to the electrons generated in the glucose-GO_x redox reaction. In the second cycle, the current decreased back to 7×10^{-11} A/μm after glucose was removed from the channel (state #1), and then it increased to 4.33×10^{-5} A/μm when glucose was sensed (state #2). Similar changes in current were also observed in the following cycle, as shown in Figure 4b. In addition, we varied the concentrations of glucose in every cycle and calculated the sensitivity values for six different cycles (Figure 4c). In the first cycle, when 1 mM of glucose was detected, the sensitivity value was 1.08×10^2 A/A, and then, the values were changed to 5.99×10^3 A/A (second cycle: 5 mM of glucose) and 4.43×10^5 A/A (third cycle: 10 mM of glucose). For the following three cycles, we varied the glucose concentration in the same order (1, 5, and 10 mM) and extracted the sensitivity values. The sensitivity values were 1.28×10^2 A/A, 5.22×10^3 A/A, and 2.88×10^5 A/A, respectively, for the 4th (1 mM), 5th (5 mM), and 6th (10 mM) cycles. Because the WSe_2 BioFET presented almost the same sensitivity values under the same concentrations of glucose for the six cycles, we expect that this device can be used repeatedly. Finally, this biosensor was compared with the previously reported devices, in terms of the biosensor type, channel material, detection molecule, sensitivity, and reusability in Supporting Information Table S1.

CONCLUSIONS

In this work, we demonstrated a highly sensitive and reusable membraneless WSe_2 BioFET. The membraneless structure was achieved by exploiting defect-free WSe_2 as the channel material, consequently magnifying the sensitivity of the WSe_2 BioFET. The sensitivity was further enhanced by creating a small number of surface defects through weak O_2 plasma treatment, which serve as extra binding sites for bioreceptor immobilization. We discovered that the O_2 plasma treatment damaged the crystallinity of WSe_2 by Raman spectroscopy and XPS analyses, thereby creating Se vacancies and W−O bonds on the surface. We also confirmed that the created surface defects enabled more APTES molecules (chemical linkers) to be attached on the WSe_2 surface. The sensing performance of the WSe_2 BioFET was investigated in detail under different concentrations of glucose by electrical measurements, where we achieved a superior sensitivity of 2.87×10^5 A/A for 10 mM glucose. In addition, the reusability of the WSe_2 BioFET was presented in repeated cycles of application and rinsing of glucose, while maintaining its high sensitivity. This study suggests an effective platform for future sensitive and reusable biosensors based on defect-free vdW materials.

ASSOCIATED CONTENT

Supporting Information

The Supporting Information is available free of charge on the ACS Publications website at DOI: 10.1021/acsami.8b03432.

Thickness of WSe_2 flake as analyzed by atomic force microscopy; I_D−V_G characteristics after rinsing process and during six cycles with different glucose concentrations; and performance comparison with other biosensors (PDF)

AUTHOR INFORMATION

Corresponding Authors

*E-mail: donghwan.jun@kanc.re.kr (D.-H.J.).
*E-mail: jhpark9@skku.edu (J.-H.P.).

ORCID

Jeong Ho Cho: 0000-0002-1030-9920
Sungjoo Lee: 0000-0003-1284-3593
Jin-Hong Park: 0000-0001-8401-6920

Author Contributions

⊥H.W.L. and D.-H.K. contributed equally. All authors have given approval to the final version of the manuscript.

Funding

The data that support the findings of this study is available from the corresponding author upon request.

Notes

The authors declare no competing financial interest.

ACKNOWLEDGMENTS

This research was supported by grants from the Gyeonggi Technology Development Program funded by Gyeonggi Province (no. 2016BB008), the Basic Research Lab Program and Basic Science Research Program through the National Research Foundation of Korea (NRF) funded by the Korea Government (MSIP) (nos. 2018R1A2A2A05020475, 2017R1A4A1015400, and 2015M3A7B7045496), and the Future Semiconductor Device Technology Development Program (10067739) funded by the Ministry of Trade, Industry & Energy (MOTIE) and the Korea Semiconductor Research Consortium (KSRC).

REFERENCES

(1) Vigneshvar, S.; Sudhakumari, C. C.; Senthilkumaran, B.; Prakash, H. Recent Advances in Biosensor Technology for Potential Applications − An Overview. *Front. Bioeng. Biotechnol.* **2016**, *4*, 11.
(2) Perumal, V.; Hashim, U. Advances in Biosensors: Principle, Architecture and Applications. *J. Appl. Biomed.* **2014**, *12*, 1−15.
(3) Luppa, P. B.; Sokoll, L. J. Immunosensors—Principles and Applications to Clinical Chemistry. *Clin. Chim. Acta* **2001**, *314*, 1−26.
(4) Malhotra, B. D.; Chaubey, A. Biosensors for Clinical Diagnostics Industry. *Sens. Actuators, B* **2003**, *91*, 117−127.
(5) Wang, J. Electrochemical Glucose Biosensors. *Chem. Rev.* **2008**, *108*, 814−825.
(6) Mehmeti, E.; Stanković, D. M.; Chaiyo, S.; Zavasnik, J.; Žagar, K.; Kalcher, K. Wiring of Glucose Oxidase with Graphene Nanoribbons: an Electrochemical Third Generation Glucose Biosensor. *Microchim. Acta* **2017**, *184*, 1127−1134.
(7) Shim, N. Y.; Bernards, D.; Macaya, D.; DeFranco, J.; Nikolou, M.; Owens, R.; Malliaras, G. All-Plastic Electrochemical Transistor for Glucose Sensing Using a Ferrocene Mediator. *Sensors* **2009**, *9*, 9896−9902.
(8) Liu, R.; Li, S.; Yu, X.; Zhang, G.; Zhang, S.; Yao, J.; Keita, B.; Nadjo, L.; Zhi, L. Facile Synthesis of Au-Nanoparticle/Polyoxometalate/Graphene Tricomponent Nanohybrids: An Enzyme-Free Electro-

DOI: 10.1021/acsami.8b03432
ACS Appl. Mater. Interfaces XXXX, XXX, XXX−XXX

chemical Biosensor for Hydrogen Peroxide. *Small* **2012**, *8*, 1398−1406.
(9) Suter, J. D.; White, I. M.; Zhu, H.; Shi, H.; Caldwell, C. W.; Fan, X. Label-Free Quantitative DNA Detection Using the Liquid Core Optical Ring Resonator. *Biosens. Bioelectron.* **2008**, *23*, 1003−1009.
(10) Noto, M.; Keng, D.; Teraoka, I.; Arnold, S. Detection of Protein Orientation on the Silica Microsphere Surface Using Transverse Electric/Transverse Magnetic Whispering Gallery Modes. *Biophys. J.* **2007**, *92*, 4466−4472.
(11) Fan, X.; White, I. M.; Shopova, S. I.; Zhu, H.; Suter, J. D.; Sun, Y. Sensitive Optical Biosensors for Unlabeled Targets: A review. *Anal. Chim. Acta* **2008**, *620*, 8−26.
(12) Nusz, G. J.; Curry, A. C.; Marinakos, S. M.; Wax, A.; Chilkoti, A. Rational Selection of Gold Nanorod Geometry for Label-Free Plasmonic Biosensors. *ACS Nano* **2009**, *3*, 795−806.
(13) do Nascimento, N. M.; Juste-Dolz, A.; Grau-García, E.; Román-Ivorra, J. A.; Puchades, R.; Maquieira, A.; Morais, S.; Gimenez-Romero, D. Label-Free Piezoelectric Biosensor for Prognosis and Diagnosis of Systemic Lupus Erythematosus. *Biosens. Bioelectron.* **2017**, *90*, 166−173.
(14) Davis, K. A.; Leary, T. R. Continuous Liquid-Phase Piezoelectric Biosensor for Kinetic Immunoassays. *Anal. Chem.* **1989**, *61*, 1227−1230.
(15) Giamblanco, N.; Conoci, S.; Russo, D.; Marletta, G. Single-Step Label-Free Hepatitis B Virus Detection by a Piezoelectric Biosensor. *RSC Adv.* **2015**, *5*, 38152−38158.
(16) Zhao, Y.; Fu, Y.; Wang, P.; Xing, L.; Xue, X. Highly Stable Piezo-Immunoglobulin-Biosensing of a SiO_2/ZnO Nanogenerator as a Self-Powered/Active Biosensor Arising from the Field Effect Influenced Piezoelectric Screening Effect. *Nanoscale* **2015**, *7*, 1904−1911.
(17) Liu, X.; Lin, P.; Yan, X.; Kang, Z.; Zhao, Y.; Lei, Y.; Li, C.; Du, H.; Zhang, Y. Enzyme-Coated Single ZnO Nanowire FET Biosensor for Detection of Uric Acid. *Sens. Actuators, B* **2013**, *176*, 22−27.
(18) Park, H.-Y.; Dugasani, S. R.; Kang, D.-H.; Yoo, G.; Kim, J.; Gnapareddy, B.; Jeon, J.; Kim, M.; Song, Y. J.; Lee, S.; Heo, J.; Jeon, Y. J.; Park, S. H.; Park, J.-H. M-DNA/Transition Metal Dichalcogenide Hybrid Structure Based Bio-FET Sensor with Ultrahigh Sensitivity. *Sci. Rep.* **2016**, *6*, 35733.
(19) Bergveld, P. Development of an Ion-Sensitive Solid-State Device for Neurophysiological Measurements. *IEEE Trans. Biomed. Eng.* **1970**, *BME-17*, 70−71.
(20) Lee, J.; Dak, P.; Lee, Y.; Park, H.; Choi, W.; Alam, M. A.; Kim, S. Two-Dimensional Layered MoS_2 Biosensors Enable Highly Sensitive Detection of Biomolecules. *Sci. Rep.* **2014**, *4*, 7352.
(21) Jamasb, S.; Collins, S.; Smith, R. L. A Physical Model for Drift in pH ISFETs. *Sens. Actuators, B* **1998**, *49*, 146−155.
(22) Pan, T.-M.; Cheng, C.-H.; Lee, C.-D. Yb_2O_3 Thin Films as a Sensing Membrane for pH-ISFET Application. *J. Electrochem. Soc.* **2009**, *156*, J108−J111.
(23) Lu, C.-H.; Hou, T.-H.; Pan, T.-M. High-Performance Double-Gate α-InGaZnO ISFET pH Sensor Using a HfO_2 Gate Dielectric. *IEEE Trans. Electron. Dev.* **2018**, *65*, 237.
(24) Kovačević, G.; Pivac, B. Structure, Defects, and Strain in Silicon-Silicon Oxide Interfaces. *J. Appl. Phys.* **2014**, *115*, 043531.
(25) Lee, K.; Nair, P. R.; Scott, A.; Alam, M. A.; Janes, D. B. Device Considerations for Development of Conductance-Based Biosensors. *J. Appl. Phys.* **2009**, *105*, 102046.
(26) Lasseter, T. L.; Clare, B. H.; Abbott, N. L.; Hamers, R. J. Covalently Modified Silicon and Diamond Surfaces: Resistance to Nonspecific Protein Adsorption and Optimization for Biosensing. *J. Am. Chem. Soc.* **2004**, *126*, 10220−10221.
(27) Yang, W.; Auciello, O.; Butler, J. E.; Cai, W.; Carlisle, J. A.; Gerbi, J. E.; Gruen, D. M.; Knickerbocker, T.; Lasseter, T. L.; Russell, J. N.; Smith, L. M.; Hamers, R. J. DNA-Modified Nanocrystalline Diamond Thin-Films as Stable, Biologically Active Substrates. *Nat. Mater.* **2002**, *1*, 253−257.
(28) Kalantar-zadeh, K.; Ou, J. Z.; Daeneke, T.; Strano, M. S.; Pumera, M.; Gras, S. L. Two-Dimensional Transition Metal Dichalcogenides in Biosystems. *Adv. Funct. Mater.* **2015**, *25*, 5086−5099.
(29) Nipane, A.; Karmakar, D.; Kaushik, N.; Karande, S.; Lodha, S. Few-Layer MoS_2 p-Type Devices Enabled by Selective Doping Using Low Energy Phosphorus Implantation. *ACS Nano* **2016**, *10*, 2128−2137.
(30) Kang, N.; Paudel, H. P.; Leuenberger, M. N.; Tetard, L.; Khondaker, S. I. Photoluminescence Quenching in Single-Layer MoS_2 via Oxygen Plasma Treatment. *J. Phys. Chem. C* **2014**, *118*, 21258−21263.
(31) Rahimnejad, S.; He, J. H.; Pan, F.; Lee, X.; Chen, W.; Wu, K.; Xu, G. Q. Enhancement of the Photocatalytic Efficiency of WO_3 Nanoparticles via Hydrogen Plasma Treatment. *Mater. Res. Express* **2014**, *1*, 045044.
(32) Park, H.-Y.; Dugasani, S. R.; Kang, D.-H.; Jeon, J.; Jang, S. K.; Lee, S.; Roh, Y.; Park, S. H.; Park, J.-H. n- and p-Type Doping Phenomenon by Artificial DNA and M-DNA on Two-Dimensional Transition Metal Dichalcogenides. *ACS Nano* **2014**, *8*, 11603−11613.
(33) Kang, D.-H.; Kim, M.-S.; Shim, J.; Jeon, J.; Park, H.-Y.; Jung, W.-S.; Yu, H.-Y.; Pang, C.-H.; Lee, S.; Park, J.-H. High-Performance Transition Metal Dichalcogenide Photodetectors Enhanced by Self-Assembled Monolayer Doping. *Adv. Funct. Mater.* **2015**, *25*, 4219−4227.
(34) Jo, S.-H.; Park, H.-Y.; Kang, D.-H.; Shim, J.; Jeon, J.; Choi, S.; Kim, M.; Park, Y.; Lee, J.; Song, Y. J.; Lee, S.; Park, J.-H. Broad Detection Range Rhenium Diselenide Photodetector Enhanced by (3-Aminopropyl)Triethoxysilane and Triphenylphosphine Treatment. *Adv. Mater.* **2016**, *28*, 6711−6718.
(35) Shim, J.; Oh, A.; Kang, D.-H.; Oh, S.; Jang, S. K.; Jeon, J.; Jeon, M. H.; Kim, M.; Choi, C.; Lee, J.; Lee, S.; Yeom, G. Y.; Song, Y. J.; Park, J.-H. High-Performance 2D Rhenium Disulfide (ReS2) Transistors and Photodetectors by Oxygen Plasma Treatment. *Adv. Mater.* **2016**, *28*, 6985−6992.
(36) Tosun, M.; Chan, L.; Amani, M.; Roy, T.; Ahn, G. H.; Taheri, P.; Carraro, C.; Ager, J. W.; Maboudian, R.; Javey, A. Air-Stable n-Doping of WSe_2 by Anion Vacancy Formation with Mild Plasma Treatment. *ACS Nano* **2016**, *10*, 6853−6860.
(37) Kang, W.-M.; Lee, S.; Cho, I.-T.; Park, T. H.; Shin, H.; Hwang, C. S.; Lee, C.; Park, B.-G.; Lee, J.-H. Multi-Layer WSe_2 Field Effect Transistor with Improved Carrier-Injection Contact by Using Oxygen Plasma Treatment. *Solid-State Electron.* **2018**, *140*, 2−7.
(38) Kalantar-zadeh, K.; Ou, J. Z.; Daeneke, T.; Mitchell, A.; Sasaki, T.; Fuhrer, M. S. Two Dimensional and Layered Transition Metal Oxides. *Appl. Mater. Today* **2016**, *5*, 73−89.

DOI: 10.1021/acsami.8b03432
ACS Appl. Mater. Interfaces XXXX, XXX, XXX−XXX